RESEARCH ARTICLE

# Severe Acute Respiratory Syndrome Coronavirus Nonstructural Proteins 3, 4, and 6 Induce Double-Membrane Vesicles

**Megan M. Angelini,[a] Marzieh Akhlaghpour,[a] Benjamin W. Neuman,[b] Michael J. Buchmeier[c]**

University of California Irvine, Department of Molecular Biology and Biochemistry, Irvine, California, USA[a]; School of Biological Sciences, University of Reading, Reading, Berkshire, United Kingdom[b]; University of California Irvine, Departments of Molecular Biology and Biochemistry and Division of Infectious Disease, Department of Medicine, Irvine, California, USA[c]

**ABSTRACT Coronaviruses (CoV), like other positive-stranded RNA viruses, redirect and rearrange host cell membranes for use as part of the viral genome replication and transcription machinery. Specifically, coronaviruses induce the formation of double-membrane vesicles in infected cells. Although these double-membrane vesicles have been well characterized, the mechanism behind their formation remains unclear, including which viral proteins are responsible. Here, we use transfection of plasmid constructs encoding full-length versions of the three transmembrane-containing nonstructural proteins (nsps) of the severe acute respiratory syndrome (SARS) coronavirus to examine the ability of each to induce double-membrane vesicles in tissue culture. nsp3 has membrane disordering and proliferation ability, both in its full-length form and in a C-terminal-truncated form. nsp3 and nsp4 working together have the ability to pair membranes. nsp6 has membrane proliferation ability as well, inducing perinuclear vesicles localized around the microtubule organizing center. Together, nsp3, nsp4, and nsp6 have the ability to induce double-membrane vesicles that are similar to those observed in SARS coronavirus-infected cells. This activity appears to require the full-length form of nsp3 for action, as double-membrane vesicles were not seen in cells coexpressing the C-terminal truncation nsp3 with nsp4 and nsp6.**

**IMPORTANCE Although the majority of infections caused by coronaviruses in humans are relatively mild, the SARS outbreak of 2002 to 2003 and the emergence of the human coronavirus Middle Eastern respiratory syndrome (MERS-CoV) in 2012 highlight the ability of these viruses to cause severe pathology and fatality. Insight into the molecular biology of how coronaviruses take over the host cell is critical for a full understanding of any known and possible future outbreaks caused by these viruses. Additionally, since membrane rearrangement is a tactic used by all known positive-sense single-stranded RNA viruses, this work adds to that body of knowledge and may prove beneficial in the development of future therapies not only for human coronavirus infections but for other pathogens as well.**

**Received** 12 July 2013 **Accepted** 16 July 2013 **Published** 13 August 2013

**Citation** Angelini MM, Akhlaghpour M, Neuman BW, Buchmeier MJ. 2013. Severe acute respiratory syndrome coronavirus nonstructural proteins 3, 4, and 6 induce double-membrane vesicles. mBio 4(4):e00524-13. doi:10.1128/mBio.00524-13.

**Editor** Anne Moscona, Weill Medical College-Cornell



Address correspondence to Michael J. Buchmeier. m.buchmeier@uci.edu.

Severe acute respiratory syndrome, or SARS, emerged as a life-threatening disease of unknown origin in late 2002 in the Guangdong Province of southern China. The disease presented as an atypical pneumonia and rapidly spread throughout Asia and on to at least 29 countries worldwide, infecting over 8,000 individuals, with an approximately 10% mortality rate. Multiple laboratory groups ultimately identified the causative agent as a novel coronavirus: the SARS coronavirus (SARS-CoV) (1–5). Although there have not been any epidemic outbreaks of the SARS-CoV since the initial incident, the recent emergence of a related deadly human coronavirus, Middle Eastern respiratory syndrome coronavirus (MERS-CoV), highlights the importance of continued research into this group of human pathogens (6–11).

Coronaviruses, members of the *Nidovirales* order, are enveloped, positive-sense, single-stranded RNA viruses (12–14). Their genome is the largest of all known RNA viruses, ranging from approximately 26 to 32 kb. The SARS coronavirus genome is 29.7 kb in size, the first two-thirds of which encompasses the overlapping open reading frames 1a and 1b (ORF1a/b) (15, 16). ORF1a/b is translated into two large polyproteins (pp): pp1a and, via a frameshift event, pp1ab (17–19). These polyproteins are co- and posttranslationally cleaved by viral proteases into the 16 nonstructural proteins (nsps) involved in viral genome replication and transcription (20, 21).

Similar to other positive-sense, single-stranded RNA viruses, coronavirus genomic replication and transcription are moderated by a large RNA replication complex that is anchored in rearranged internal host membranes (22–29). These membranes act as a framework for viral genome replication by localizing and concentrating the necessary factors and possibly providing protection from host cell defenses. The hallmark membrane rearrangements observed upon coronavirus infection are double-membrane vesicles (DMVs), named for their distinctive double-lipid bilayer as seen in electron micrographs. These DMVs are found in conjunction with reticular regions of a convoluted membrane (CM) between them, and contiguity with the endoplasmic reticulum (ER)

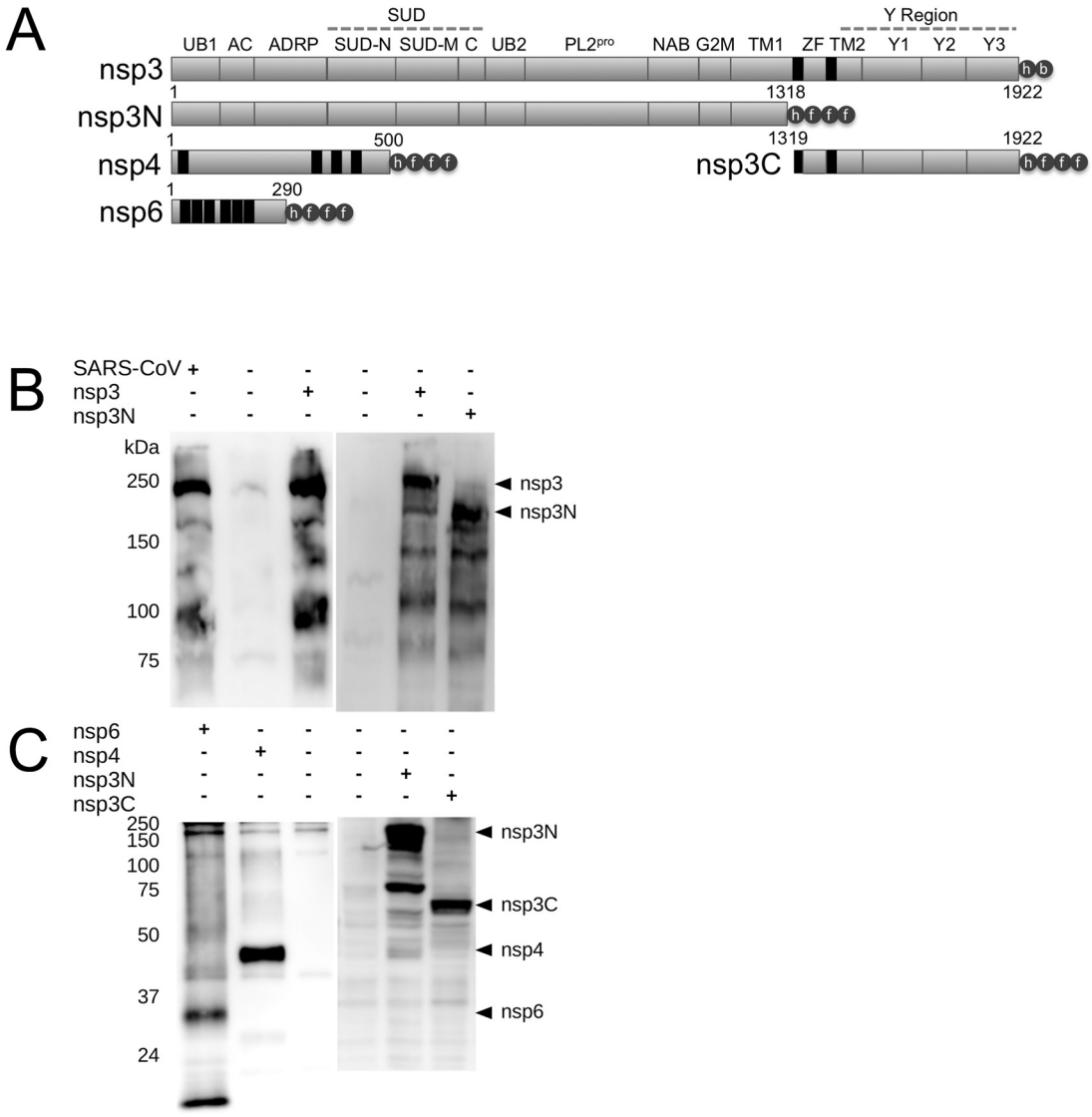


**FIG 1** Expression of SARS-CoV nonstructural proteins. (A) Schematic of nsp3, nsp3N, nsp3C, nsp4, and nsp6 constructs used. UB1, ubiquitin-like domain 1; AC, acidic region; ADRP, ADP-ribose-1′′-phosphatase; SUD, SARS unique domain; UB2, ubiquitin-like domain 2; PLP2$^{PRO}$, papain-like protease; NAB, nucleic acid binding domain; G2M, group II-specific marker; TM, transmembrane region; ZF, putative metal-binding region; Y, Y region; h, HA epitope tag; b, biotinylation signal sequence; f, FLAG epitope tag. (B) Left panel: detection of nsp3 in SARS-CoV-infected cell lysate and nsp3-transfected cell lysate via anti-nsp3. Right panel: detection of nsp3 and nsp3N in transfected cell lysates via anti-nsp3. (C) Detection of nsp4, nsp6, nsp3N, and nsp3C in transfected cell lysates via anti-FLAG.

has been observed in electron microscopy (EM) despite a lack of canonical ER membrane markers (30–35). Certain subsets of the coronavirus replication machinery have been shown to move in the cell in a manner that corresponds with microtubule-associated transport, but microtubule disruption does not have an effect on viral genome replication levels (32). Although much has been done to study coronavirus-induced DMVs, it remains unclear which specific viral proteins are responsible for their induction and which host cellular membranes or processes are engaged (29, 36–39).

The nsps, also referred to as the replicase proteins, localize to the DMVs and CMs (33). These vesicles, together with their localized proteins, are referred to as the "replication-transcription complex" (RTC). It has been seen for another group of the *Nidovirales*, the arteriviruses, that two nonstructural proteins alone were sufficient to induce double-membrane vesicles (40–42). The two arterivirus nsps responsible for membrane rearrangement are related to SARS-CoV nsp3 and nsp4, which contain transmembrane domains. Additionally, SARS-CoV has a third integral membrane nonstructural protein, nsp6 (43, 44). SARS-CoV nsp3 is a 215-kDa, transmembrane, glycosylated, multidomain protein that has been shown to interact with numerous other proteins involved in replication and transcription and, as such, may serve as a scaffolding protein for these processes (45–49). nsp4 has been shown to cause aberrant DMV formation upon mutation, leading to a loss of nsp4 glycosylation (50–54). nsp6 has been shown to activate autophagy, inducing vesicles containing Atg5 and LC3-II (55). Expression of a construct encoding the last one-third of nsp3

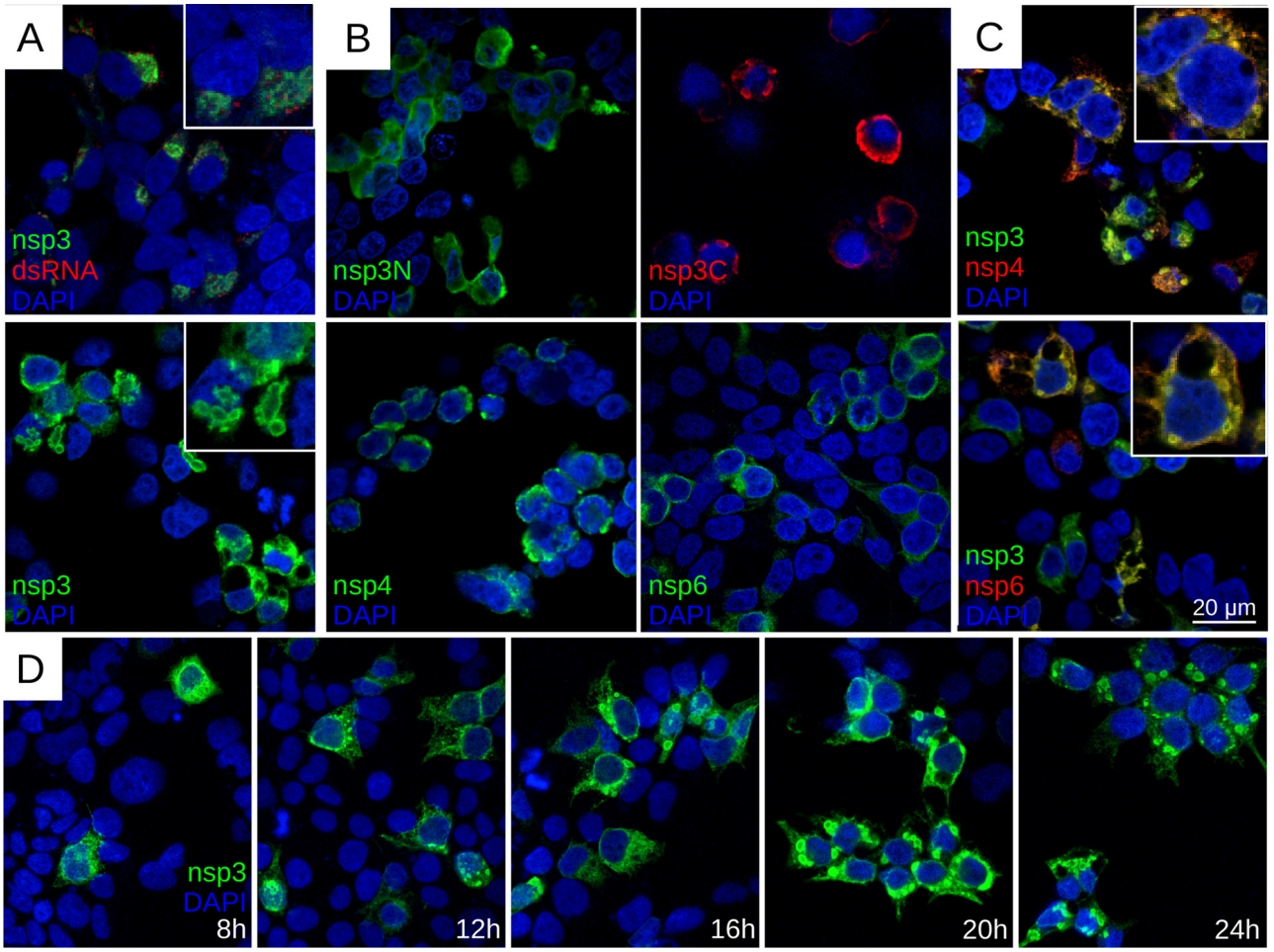


**FIG 2** Intracellular localization of accumulation of SARS-CoV nonstructural proteins. (A) Upper panel: detection of nsp3 (green) and double-stranded RNA (dsRNA) (red) in SARS-CoV-infected HEK293T-ACE2 cells (MOI = 0.1, fixed 24 h postinfection [hpi]). Lower panel: detection of nsp3 (green) in nsp3-transfected HEK293T cells. (B) Detection of nsp3N (green), nsp3C (red), nsp4 (green), and nsp6 (green) in transfected HEK293T cells using anti-FLAG antibody. (C) Upper panel: detection of nsp3 (green) and nsp4 (red) in cotransfected HEK293T cells. Lower panel: detection of nsp3 (green) and nsp6 (red) in cotransfected HEK293T cells. (D) Time course experiment detecting nsp3 (green) in transfected cells (fixed at the indicated time points) over a 24-h period.

with nsp4 suggested interaction of these two proteins via their ability to relocalize each other in immunofluorescence imaging (31). In these coexpressing cells, nsp6 was also relocalized (14). nsp6 has also been shown to interact with a truncated N-terminal region of nsp3 via yeast two-hybrid assays (46).

In this study, using both confocal and electron microscopy, we examined the ability of SARS-CoV nsp3, nsp4, and nsp6 to induce double-membrane vesicles via transfection.

## RESULTS

**Expression of SARS-CoV nsp3, nsp4, and nsp6.** To determine if any of the three integral membrane nonstructural proteins of the SARS-CoV are capable of inducing double-membrane vesicles, we first validated the expression of our various nsp3, nsp4, and nsp6 constructs via Western blot analysis. Constructs were created (Fig. 1A) as described previously (56). Lysates from HEK293T cells transfected with our full-length nsp3 construct, termed nsp3 and featuring a C-terminal hemagglutinin (HA) tag followed by a tobacco etch virus (TEV) cleavage site and a biotinylation signal, yield a pattern similar to that seen with SARS-CoV-infected cell lysates when probed using an anti-nsp3 antibody (Fig. 1B). A truncated form of nsp3 (N terminus through the group II-specific marker [GSM] domain), called nsp3N, was also detectable using an anti-nsp3 antibody (Fig. 1B). Our nsp3N-terminal construct, nsp3C-terminal construct (spanning the first transmembrane domain through the C terminus), nsp4 construct, and nsp6 construct, all featuring a C-terminal HA tag followed by a 3× FLAG tag, are detectable using an anti-FLAG antibody (Fig. 1C). We note here that the nsp3C-terminal construct that we used is distinct from that used by Hagemeijer et al. (32) mentioned in the introduction, which included the GSM domain. Immunofluorescence detection of all constructs was also performed (Fig. 2).

Phenotypes observed in electron microscopy of transfected samples were categorized and can be found in Table 1. A comparison of our observed results versus expected results can be found in Table 2. An explanation of the quantitation methods used for both tables can be found in Materials and Methods.

**Both full-length and truncated forms of nsp3 induce DMB and MGV.** Single transfection of both full-length nsp3 and nsp3C yielded similar phenotypes. Both appeared capable of causing the

**TABLE 1** Raw number of cells counted that contained a given phenotype compared to total number of cells counted

| Transfected | Total no. of cell sections | No. (%) of cell sections showing at least one instance of each phenotype[a] | | | | | | | | |
|---|---|---|---|---|---|---|---|---|---|---|
| | | Normal | DMB | MGV | DMB with MGV | MTOCV | MLB | DMB and MTOCV | MLB and MTOCV | DMV cluster |
| None | 269 | 269 (100) | No | No | No | No | No | No | No | No |
| nsp3 | 170 | 147 (86) | 7 (4) | 6 (4) | 4 (2) | 5 (3) | No | 1 (1) | No | No |
| nsp3C | 217 | 201 (93) | 4 (2) | 9 (4) | No | 3 (1) | No | No | No | No |
| nsp3N | 102 | 101 (99) | No | No | No | 1 (1) | No | No | No | No |
| nsp4 | 186 | 186 (100) | No | No | No | No | No | No | No | No |
| nsp6 | 218 | 181 (83) | No | No | No | 37 (17) | No | No | No | No |
| nsp3 + nsp4 | 424 | 358 (84) | 13 (3) | 6 (1) | 1 (<1) | 1 (<1) | 45 (11) | No | No | No |
| nsp3 + nsp6 | 220 | 171 (78) | 8 (4) | No | No | 36 (16) | No | 5 (2) | No | No |
| nsp4 + nsp6 | 359 | 350 (97) | No | No | No | 9 (3) | No | No | No | No |
| Nsp3 + nsp4 + nsp6 | 613 | 512 (84) | 4 (1) | No | No | 16 (3) | 61 (10) | No | 15 (2) | 5 (1) |
| nsp3C + nsp4 + nsp6 | 220 | 184 (84) | 4 (2) | 21 (10) | No | 9 (4) | No | 2 (1) | No | No |

[a] Normal, encompassing the spectrum of phenotypes not listed elsewhere in this table; No, phenotype not observed in any of the cell sections examined.

formation of large areas of disordered membrane (DMB) (Fig. 3A and C) as well as causing regions of proliferated membrane featuring multilamellar and giant vesiculation (MGV) (Fig. 3B and D). DMB differs from the classical SARS-induced convoluted membranes (CM) in that the DMB appears in larger masses without defined order or structure, often appearing as large tangled regions of membrane (Fig. 3A and C [insets]). nsp3- and nsp3C-induced DMB and MGV appeared similar, with the full-length nsp3 showing larger regions of hollow structures of nsp3 in immunofluorescence (Fig. 2A [lower panel, inset region]). These structures appear perinuclear, similar to nsp3 localization in SARS-CoV-infected cells (Fig. 2A). In a time course immunofluorescence experiment, the nsp3 hollow structures grew larger as time progressed, with the hollow centers being first visible at 12 h posttransfection (Fig. 2D). The nsp3N construct appeared to be dispersed throughout the cytoplasm in immunofluorescence (Fig. 2B) and showed no distinct phenotype in electron microscopy.

**Nsp4 with nsp3 produces MLBs featuring double-membrane walls.** Transfection of nsp4 alone induced a punctate pattern as observed via immunofluorescence microscopy consistent with the localization of nsp4 to the ER (Fig. 2B), as others have demonstrated (31, 52). In electron microscopy, cells transfected with nsp4 alone showed no distinct phenotype (Table 1). Cotransfection of nsp3 and nsp4 produced a pattern that was distinct from that seen for either nsp3 alone or nsp4 alone in immunofluorescence (Fig. 2C). In electron microscopy, it was observed that the membranes in this cotransfection form an extensive (typically ~2-$\mu$m diameter) winding maze-like body (MLB), featuring paired membranes interspersed with double-membrane circular structures with an average diameter of ~80 nm (Fig. 4). The apposing walls of the MLB were typically separated from each other by approximately 20 nm. The MLB appear perinuclear, and interconnections with the ER were present (Fig. 4, black arrowheads).

**Nsp6 induces single-membrane vesicles around microtubule organizing centers.** Transfection of nsp6, either alone or along with nsp3, yielded the presence of a large amount of smooth-walled single-membrane spherical vesicles approximately 280 ± 60 nm in diameter (Fig. 5C). While this microtubule organizing

**TABLE 2** Observed frequency of nsp-related intracellular features compared to the expected frequency

| Transfected | Phenotype observed[a] | Expected transfection efficiency (%)[b] | Approximate diam ($\mu$m) | Expected frequency (%)[c] | Observed frequency (%) |
|---|---|---|---|---|---|
| nsp3 | DMB/MGV | 70 | 4 | 19 | 11 |
| nsp3C | DMB/MGV | 70 | 4 | 19 | 6 |
| nsp6 | MTOCV | 70 | 4 | 19 | 17 |
| nsp3 + nsp4 | DMB/MGV | 21 | 4 | 6 | 5 |
| | MLB | 49 | 2 | 7 | 11 |
| nsp3 + nsp6 | DMB/MGV | 70 | 4 | 19 | 4 |
| | MTOCV | 70 | 4 | 19 | 18 |
| nsp4 + nsp6 | MTOCV | 21 | 4 | 6 | 3 |
| nsp3 + nsp4 + nsp6 | DMB/MGV | 21 | 4 | 6 | 1 |
| | MTOCV | 21 | 4 | 6 | 5 |
| | MLB | 15 | 2 | 2 | 12 |
| | DMV cluster | 34 | 0.5 | 1 | 1 |
| nsp3C + nsp4 + nsp6 | DMB/MGV | 70 | 4 | 9 | 13 |
| | MTOCV | 54 | 4 | 7 | 6 |

[a] Both nsp3-induced membrane phenotypes are combined under the heading DMB/MGV.

[b] Data are based on an assumed independent 70% transfection efficiency for each plasmid, combining probabilities for plasmid combinations expected to result in the given phenotype; e.g., in nsp3-nsp6 transfection, the nsp6 phenotype is expected in nsp6 single transfectants (21% of cells) plus nsp3-nsp6 double transfectants (49% of cells) because nsp3 and nsp6 phenotypes appear to be independent, whereas nsp4-nsp6 transfection would be expected to result only in the nsp6 phenotype in nsp6 single transfectants (21% of cells) because nsp4 appeared to counteract the nsp6 phenotype.

[c] Calculated as expected transfection efficiency × (average diameter of feature/15-$\mu$m average cell diameter).

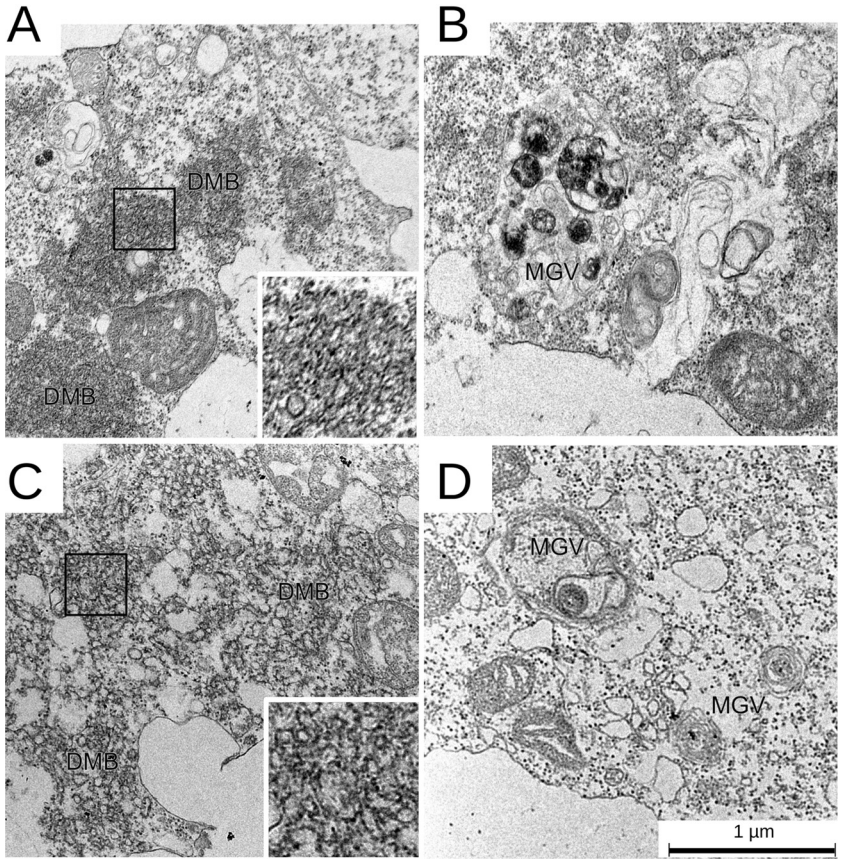


**FIG 3** Disordered membrane body (DMB) and multilamellar and giant vesiculation (MGV) in SARS-CoV nsp3- and nsp3C-transfected cells. (A) DMB in nsp3-transfected cell. Zoomed region shows membrane detail. (B) MGV in nsp3-transfected cell. (C) DMB in nsp3C-transfected cell. Zoomed region shows membrane detail. (D) MGV in nsp3C-transfected cell.

center vesiculation (MTOCV) phenotype was not exclusive to nsp6 transfections, it was far more prevalent in nsp6-transfected cells (Table 1). This was consistent with what we observed in immunofluorescence with single nsp6 transfections, where the nsp6 signals clustered perinuclearly in one area of the cell. Interestingly, when nsp6 was coexpressed with nsp4, the MTOCV phenotype was lost (Fig. 5D) and regions surrounding the MTOC instead looked like the equivalent areas in untransfected or nsp4 singly transfected cells (Fig. 5A and B) (Table 1).

**Nsp3, nsp4, and nsp6 together induce a pattern of double-membrane vesicles similar to that seen in SARS-CoV-infected cells.** A triple transfection of nsp3 and nsp4 and nsp6 yielded double-membrane vesicles (Fig. 6C to E) with connections to convoluted membranes of morphology similar to that of those induced in SARS coronavirus-infected cells (Fig. 6A and B). Whereas SARS-CoV-induced DMVs tend to remain approximately 210 ± 30 nm in diameter, the DMVs induced by nsp3, nsp4, and nsp6 triple transfection exhibited a smaller average diameter of 120 ± 40 nm. Both infection-induced and transfection-induced DMVs showed an approximate 20-nm separation between apposing membranes. As is the case for SARS-induced DMVs, the triple transfection induced interconnected DMVs that appeared perinuclear, showed contiguity with the ER, and exhibited dark membrane staining. In addition to the DMVs induced by the triple transfection, regions of MLB and MTOCV appearing in the same cell were found three times as frequently as DMVs were found. Interestingly, a triple transfection of nsp3C with nsp4 and nsp6 yielded regions of DMB, MGV, and MTOCV but never maze-like bodies, double-membrane vesicles, or any additional novel structures (Table 1).

## DISCUSSION

Although it is understood that viral replicase interaction with host membranes is a requirement for successful coronavirus infection, it has not yet been made clear which viral proteins are involved in double-membrane vesicle formation and the nature of the cellular organelles that are compromised. In this study, we used immunofluorescence and electron microscopy to examine the ability of the three membrane-spanning nonstructural proteins of the SARS coronavirus to induce double-membrane vesicles via transfection. We found that exogenous nsp3 alone, both full length and the C-terminal transmembrane-containing region, was capable of inducing DMB as well as regions of MGV, suggesting a role for the C terminus of nsp3 in membrane production or expansion of existing membranes. In immunofluorescence time course experiments, nsp3 induced hollow accumulations that grew larger in size as time progressed posttransfection, eventually producing patterns much larger than the nsp3 signal observed in SARS-infected cells. These enlarged accumulations further support the idea of a role for nsp3 in membrane proliferation. It is interesting to note

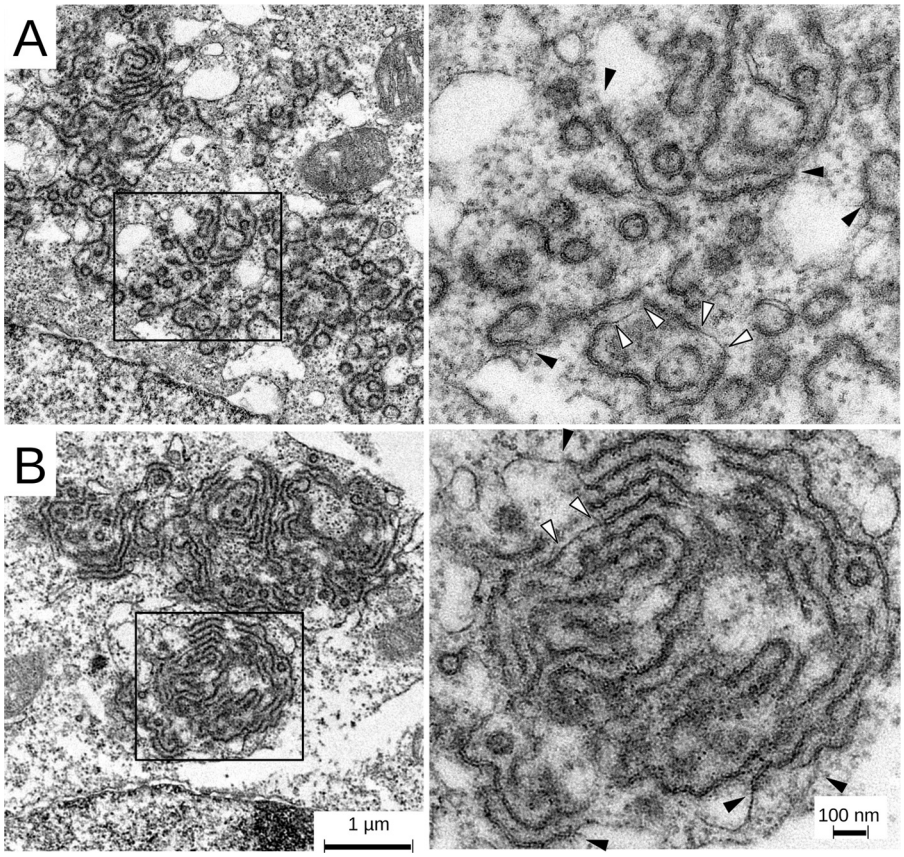


**FIG 4** Maze-like body (MLB) formation in SARS-CoV nsp3-nsp4-cotransfected cells. (A and B) Perinuclear localization and double-wall highlights (zoomed region). Interconnections to the endoplasmic reticulum (black arrowheads) and smooth-sided single membranes interrupting maze-like bodies (white arrowheads) are indicated.

that the addition of either nsp4 or nsp6 with nsp3 reduces the appearance of the MGV phenotype but not the DMB phenotype, suggesting a regulatory role of these two nsps on nsp3's membrane proliferation ability.

Cotransfection of nsp3 with nsp4 showed a dramatic effect on membrane conformation, creating a perinuclear double-membrane walled maze-like body. The MLBs in our electron micrographs consist of roughly parallel rows spaced apart by approximately 80 nm and interspersed with double-membrane walled circular structures of about 80-nm diameter, suggesting that the rows and circles are longitudinal and cross sections of closely packed double-membrane walled tubules. Electron tomography studies would prove beneficial in this determination. The MLB produced by SARS nsp3 and nsp4 is distinct from what has been shown for arteriviruses, where the arterivirus homologues of coronavirus nsp3 and nsp4 are sufficient to induce complete DMVs that look like those of arterivirus-infected cells (41). These results suggest that a biologically meaningful interaction occurs between nsp3 and nsp4, corroborating previously published data showing interactions between nsp3 and nsp4 via mammalian two-hybrid assays (Pan et al.) and Venus reporter fluorescence assays (Hagemeijer et al.) (31, 57). There is immunofluorescence evidence that a truncated protein running from the GSM to nearly the C terminus of mouse hepatitis virus (MHV) nsp3 is able to change the localization of fluorescently tagged nsp4 to form perinuclear protein clusters (31), which were not investigated further but which may be similar to the nsp3-nsp4 maze-like bodies described here. If that is the case, then the determinants of nsp3-nsp4 interaction that lead to membrane pairing would be expected to lie in the relatively poorly conserved region between the start of the GSM domain and the amino-terminal transmembrane helix of nsp3. Further research is needed to investigate the determinants of nsp3-nsp4 interaction which result in membrane pairing.

Nsp6 alone induces small spherical vesicles featuring single membranes, which cluster around the microtubule organizer center. This MTOCV phenotype is mostly lost upon addition of nsp4. This apparent counteractive effect of nsp4 on the nsp6 MTOCV phenotype cannot simply attributed to a reduced presence of nsp6 under double-transfection conditions because no reduction in MTOCV was observed in nsp3-nsp6 cotransfection. It would appear that nsp4 has a suppressive or negative effect on this phenotype or that nsp4 is relocalizing nsp6 to an area of the cell away from the MTOC. Previous studies of coronavirus RTCs have shown that certain members of the complex may traffic in the cell in a microtubule-dependent manner; however, microtubule integrity is not required for productive infection (32). Additionally, nsp6 expression may be disrupting Golgi vesicular transport mechanisms. Knockdown of RAB and ARF GTPases involved in Golgi trafficking has been shown to cause vesicle accumulation around centrioles in Drosophila (58, 59). It has been shown that MHV replication is dependent on activation of ARF1, although it

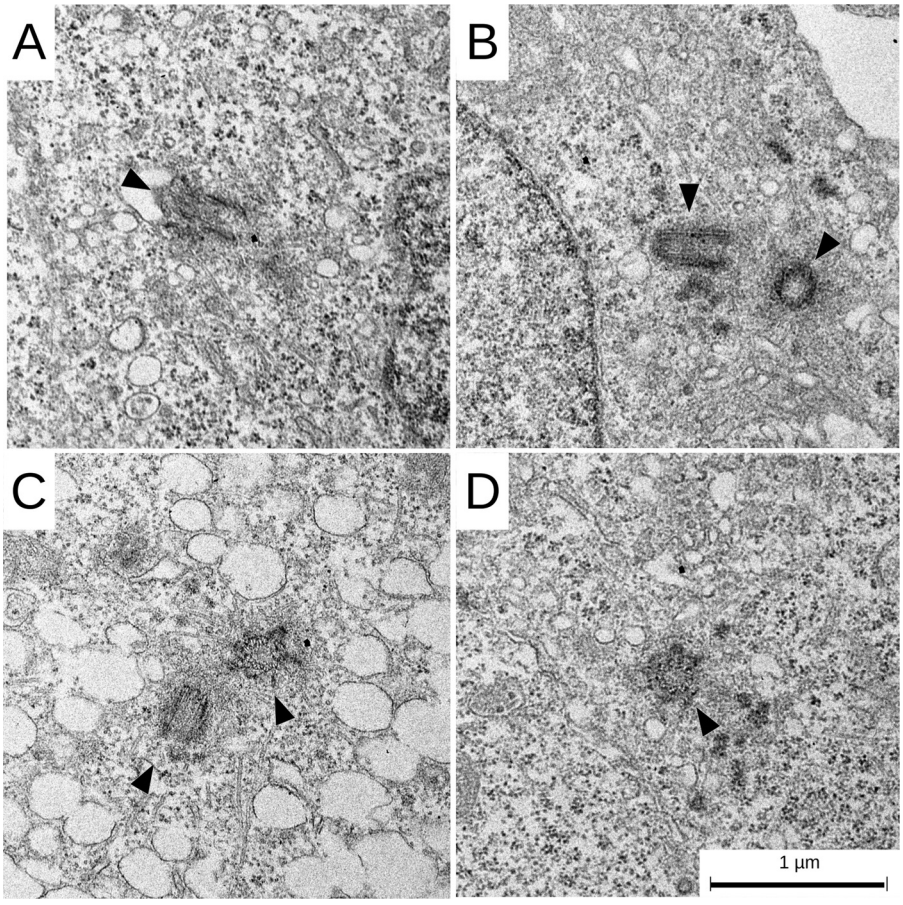


**FIG 5** Microtubule organizing center vesiculation (MTOCV) in SARS-CoV nsp6-transfected cells. (A) Untransfected control. (B) SARS-CoV nsp4-transfected cell. (C) SARS-CoV nsp6-transfected cell featuring MTOCV. (D) SARS-CoV nsp4-nsp6-cotransfected cell. Centrioles (black arrowheads) are indicated.

remains unclear whether this is related to the intracellular phenotype induced by nsp6 (60).

Triple transfection of nsp3, nsp4, and nsp6 produced formations that looked very similar to the DMVs seen in coronavirus-infected cells, with double-membrane vesicles surrounding a central convoluted membrane structure (29, 33, 35). nsp6 appears to either break up or prevent the formation of the elongated stretches of double-membrane walls seen in the nsp3-nsp4 cotransfection mazes, leaving double-membrane vesicles and regions of convoluted membrane that are consistent with SARS-CoV-infected DMVs. Triply transfected cells containing both MLB and MTOCV were about three times as frequent as cells containing DMVs (Table 1). Additionally, all cells from the triple transfection containing DMVs also contained evidence of MLBs and MTOCVs. This suggests that DMV formation from expressed nsp3, nsp4, and nsp6 is not particularly efficient. The presence of the MLBs and MTOCVs in DMV-containing cells further suggests that nsp3 and nsp4 interact more readily in this expression system than nsp4 and nsp6, which would result in loss of the MTOCV phenotype. Complementation studies using temperature-sensitive mutants of MHV have suggested that nsp4 through nsp10 may have functions in polyprotein forms prior to cleavage or that they are assembled into the RTC and then cleaved (18). The polyprotein may have a role in keeping nsp4 and nsp6 in close proximity, allowing more efficient DMV formation than in our expression system. Note that even though our nsp3C produced phenotypes very similar to those seen with the full-length nsp3 in single transfections, a triple transfection of nsp3C with nsp4 and nsp6 was unable to produce double-membrane vesicles. One explanation for the differences observed when using full-length nsp3 versus nsp3C is that the transmembrane domains, or domains C terminal to the transmembrane domains, may be responsible for membrane proliferation and convolution but some domain N terminal to the first transmembrane region of nsp3 is required for membrane pairing and regulation for the formation of DMVs. Since nsp6 was previously shown to interact with an N-terminal truncation of nsp3 via yeast two-hybrid screen, it is possible that this interaction is the critical missing link for DMV formation in the nsp3C-nsp4-nsp6 transfection (46).

A possible explanation for DMV formation is that nsp3 is responsible for membrane proliferation that results in enough membrane to form the network of DMVs that is required for RTC formation. The 20-nm distance typically found between the apposing membranes in SARS-CoV-induced DMVs and CMs was the same for nsp3-nsp4-nsp6 transfection-induced DMVs and CMs. This 20-nm distance was also found in nsp3-nsp4 MLBs, suggesting that nsp3 and nsp4 together are responsible for the DMV-like membrane pairing of the triple transfection. nsp3-nsp4 MLBs may represent a more organized version of SARS-CoV-induced convoluted membrane. The role of nsp6 may be to force

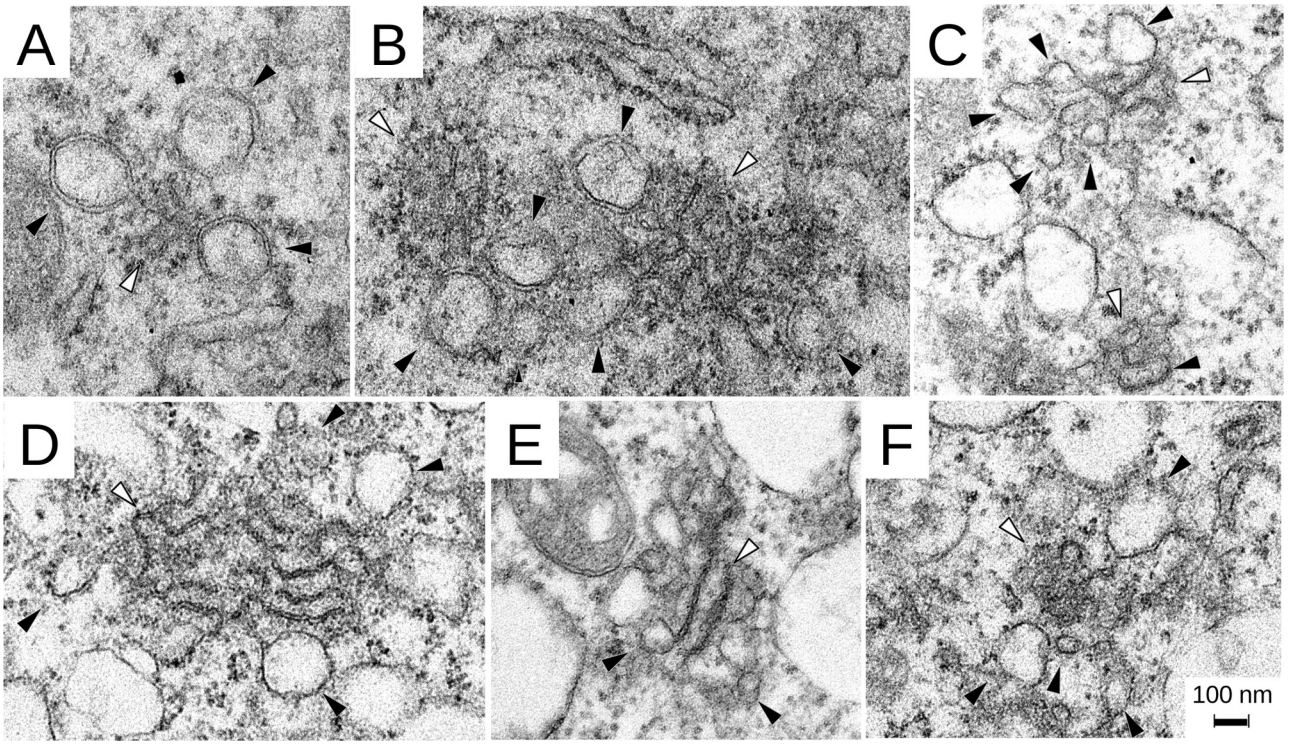


**FIG 6** SARS-CoV-induced DMVs versus triple-transfection SARS-CoV nsp3-nsp4-nsp6-induced DMVs. (A and B) SARS-CoV-infected cells. MOI = 1, fixed 7 h postinfection. (C to F) nsp3-nsp4-nsp6-transfected cells. Clusters consisting of convoluted membrane tubules (white arrowheads) ending in double-membrane vesicles (black arrowheads) are indicated.

the double-membrane structures mainly toward the formation of spherical vesicles as opposed to the MLBs seen in the absence of nsp6. These nsp6-induced structures appear to be consistent with what has been shown previously regarding the role of nsp6 in inducing autophagosomes (55). Since cleavage of nsp3 and nsp4 occurs very rapidly upon polyprotein production and nsp6 cleavage may be comparatively delayed, one possibility for DMV formation could be that the MLBs and MTOCVs form in the cell somewhat independently and then rapidly meet to produce the DMVs (20, 61). However, the presence of all three at once may directly lead to production of DMVs without any of the intermediate structures. While the DMVs that are produced by nsp3-nsp4-nsp6 transfection are similar in structure and organization to authentic SARS-induced DMVs, they are smaller. This suggests a role for other proteins or the presence of viral RNA in determining DMV size.

The precise mechanism by which each of these nsps works to produce double-membrane vesicles is a topic for future study and is likely influenced by a variety of factors, including each nsp's production from the initial polyprotein precursor, how these nsps recruit and exploit host cell proteins, and the interaction of each nsp with other viral proteins and host cell proteins.

## MATERIALS AND METHODS

**Cells and virus.** HEK293T human embryonic kidney epithelial cells (ATCC CRL-11268) were used for transfection experiments. HEK293T-ACE2 cells, which stably express the ACE2 receptor, were used for infection experiments. Cells were maintained in Dulbecco's modified Eagle's medium (HyClone) supplemented with 10% fetal bovine serum (FBS) and 1% penicillin-streptomycin. The Tor2 strain of SARS coronavirus was used for all infection experiments. Infections were performed at indicated multiplicities of infection (MOIs) for the indicated time lengths. All SARS-CoV work was performed under conditions of biosafety level 3 (BSL3) containment at the University of California, Irvine.

**Antibodies.** The primary antibodies used were rabbit anti-nsp3 (Rockland) and mouse anti-FLAG (Sigma). Alexafluor-488- and Alexafluor-594-conjugated secondary antibodies (Invitrogen) were used for immunofluorescence. Horseradish peroxidase (HRP)-conjugated secondary antibodies (Jackson Laboratories) were used for Western blotting.

**Plasmids and transfection.** All plasmids used were created as previously described using a Gateway expression system (Invitrogen) (56). Briefly, all constructs had a modified pCAGGs backbone containing a Woodchuck hepatitis virus posttranscriptional regulatory element (WPRE) and were C-terminally tagged with either an HA tag sequence followed by a tobacco etch virus (TEV) cleavage site and a biotinylation signal sequence (HA-Bio) or an HA tag sequence followed by a 3× FLAG tag sequence (HA-3×FLAG). Transfections were conducted using Lipofectamine 2000 (Invitrogen) per the manufacturer's protocol.

**Immunofluorescence assays.** HEK293T cells were grown on poly-L-lysine-coated coverslips, transfected, and fixed 24 h posttransfection using 3.7% paraformaldehyde, permeabilized with 0.1% Triton X-100, and mounted with DAPI (4′,6-diamidino-2-phenylindole) Fluoromount D (Southern Biotech). Confocal microscopy was performed with a Nikon Eclipse Ti confocal microscope. Images were processed using NIS Elements software.

**Western blotting assays.** HEK293T cells were grown in 6-well plates and lysed 24 h posttransfection using either radioimmunoprecipitation assay (RIPA) or 1% NP-40 lysis buffer with 1× protease inhibitor cocktail (Research Products International Corp). Lysates were subjected to SDS-PAGE and transferred to a polyvinylidene difluoride (PVDF) membrane for immunoblotting.

**Electron microscopy and phenotype quantification.** Cells were grown in T-75 flasks, transfected, fixed 24 h posttransfection, and harvested with 2% EM-grade glutaraldehyde in 0.1 M sodium cacodylate buffer for at least 4 h, postfixed in 1% osmium tetroxide–0.1 M cacodylate buffer for 1 h, and stained in 2% uranyl acetate en bloc for 1 h. Samples were dehydrated in ethanol, embedded in epoxy resin, sectioned at intervals of 50 to 60 nm on a Leica UCT ultramicrotome, and picked up on Formvar and carbon-coated copper grids. Sections were stained with 2% uranyl acetate for 5 min and with Sato's lead stain for 1 min. Grids were viewed using either a Tecnai $G^2$ Spirit BioTWIN transmission electron microscope equipped with an Eagle 4k high-sensitivity (HS) digital camera (FEI, Hillsboro, OR) or a Phillips CM-20 camera equipped with a 2k charge-coupled device (CCD).

Percentages found in Table 1 are based on the raw number of cells counted that contained a given phenotype compared to total number of cells counted. Table 2 compares the observed frequency of nsp-related intracellular features to the expected frequency based on the size of the feature relative to the size of the cell and the number of plasmids required to produce the feature. The estimate assumes an independent 70% transfection rate for each plasmid and an average cell diameter of 15 $\mu$m. Expected frequencies were calculated as transfection efficiency times the ratio of feature size to cell size. Expected frequencies were summed for combinations that would produce the same feature.

## ACKNOWLEDGMENTS

We thank members of the UCSD School of Medicine-Cellular & Molecular Medicine Electron Microscopy Facility, especially Timo Meerloo and Ying Jones, for aid in sample preparation, training, and microscope use for electron microscopy studies. We thank Thomas Gallagher for providing us with HEK293T-ACE2 cells. We thank Cromwell T. Cornillez-Ty for his work in plasmid creation.

Support for this work was provided by National Institutes of Health grant 5T32AI007319-23 as well as the California Center for Antiviral Drug Discovery MRPI (143226) and NIAID grant AI059799 and contract HHSN266200400058C.

## REFERENCES

1. **Drosten C, Günther S, Preiser W, van der Werf S, Brodt HR, Becker S, Rabenau H, Panning M, Kolesnikova L, Fouchier RA, Berger A, Burguière AM, Cinatl J, Eickmann M, Escriou N, Grywna K, Kramme S, Manuguerra JC, Müller S, Rickerts V, Stürmer M, Vieth S, Klenk HD, Osterhaus AD, Schmitz H, Doerr HW.** 2003. Identification of a novel coronavirus in patients with severe acute respiratory syndrome. N. Engl. J. Med. **348:**1967–1976.
2. **Ksiazek TG, Erdman D, Goldsmith CS, Zaki SR, Peret T, Emery S, Tong S, Urbani C, Comer JA, Lim W, Rollin PE, Dowell SF, Ling AE, Humphrey CD, Shieh WJ, Guarner J, Paddock CD, Rota P, Fields B, DeRisi J, Yang JY, Cox N, Hughes JM, LeDuc JW, Bellini WJ, Anderson LJ, SARS Working Group.** 2003. novel coronavirus associated with severe acute respiratory syndrome. N. Engl. J. Med. **348:**1953–1966.
3. **Pfefferle S, Schöpf J, Kögl M, Friedel CC, Müller MA, Carbajo-Lozoya J, Stellberger T, von Dall'armi E, Herzog P, Kallies S, Niemeyer D, Ditt V, Kuri T, Züst R, Pumpor K, Hilgenfeld R, Schwarz F, Zimmer R, Steffen I, Weber F, Thiel V, Herrler G, Thiel HJ, Schwegmann-Wessels C, Pöhlmann S, Haas J, Drosten C, von Brunn A.** 2011. The SARS-coronavirus-host interactome: identification of cyclophilins as target for pan-coronavirus inhibitors. PLOS Pathog. **7:**e1002331. http://dx.doi.org/10.1371/journal.ppat.1002331.
4. **Poutanen SM, Low DE, Henry B, Finkelstein S, Rose D, Green K, Tellier R, Draker R, Adachi D, Ayers M, Chan AK, Skowronski DM, Salit I, Simor AE, Slutsky AS, Doyle PW, Krajden M, Petric M, Brunham RC, McGeer AJ, National Microbiology Laboratory, Canada, Canadian Severe Acute Respiratory Syndrome Study Team.** 2003. Identification of severe acute respiratory syndrome in Canada. N. Engl. J. Med. **348:**1995–2005.
5. **Centers for Disease Control and Prevention (CDC).** 2003. Update: outbreak of severe acute respiratory syndrome—worldwide, 2003. MMWR Morb. Mortal. Wkly. Rep. **52:**269–272.
6. **Perlman S, Zhao J.** 2013. Human coronavirus EMC is not the same as severe acute respiratory syndrome coronavirus. MBio **4**(1):e00002-13. http://dx.doi.org/10.1128/mBio.00002-13.
7. **van Boheemen S, de Graaf M, Lauber C, Bestebroer TM, Raj VS, Zaki AM, Osterhaus AD, Haagmans BL, Gorbalenya AE, Snijder EJ, Fouchier RA.** 2012. Genomic characterization of a newly discovered coronavirus associated with acute respiratory distress syndrome in humans. MBio **3**(6):e00473-12. http://dx.doi.org/10.1128/mBio.00473-12.
8. **Zaki AM, van Boheemen S, Bestebroer TM, Osterhaus AD, Fouchier RA.** 2012. Isolation of a novel coronavirus from a man with pneumonia in Saudi Arabia. N. Engl. J. Med. **367:**1814–1820.
9. **Chan JF, Li KS, To KK, Cheng VC, Chen H, Yuen KY.** 2012. Is the discovery of the novel human betacoronavirus 2c EMC/2012 (HCoV-EMC) the beginning of another SARS-like pandemic? J. Infect. **65:**477–489.
10. **de Groot RJ, Baker SC, Baric RS, Brown CS, Drosten C, Enjuanes L, Fouchier RA, Galiano M, Gorbalenya AE, Memish Z, Perlman S, Poon LL, Snijder EJ, Stephens GM, Woo PC, Zaki AM, Zambon M, Ziebuhr J.** 2013. Middle East respiratory syndrome coronavirus (MERS-CoV); announcement of the Coronavirus Study Group. J. Virol. **87:**7790–7792.
11. **Josset L, Menachery VD, Gralinski LE, Agnihothram S, Sova P, Carter VS, Yount BL, Graham RL, Baric RS, Katze MG.** 2013. Cell host response to infection with novel human coronavirus EMC predicts potential antivirals and important differences with SARS coronavirus. MBio **4**(3):e00165–13. http://dx.doi.org/10.1128/mBio.00165-13.
12. **Sawicki SG, Sawicki DL, Siddell SG.** 2007. A contemporary view of coronavirus transcription. J. Virol. **81:**20–29.
13. **Ziebuhr J.** 2004. Molecular biology of severe acute respiratory syndrome coronavirus. Curr. Opin. Microbiol. **7:**412–419.
14. **Hagemeijer MC, Rottier PJ, de Haan CA.** 2012. Biogenesis and dynamics of the coronavirus replicative structures. Viruses **4:**3245–3269.
15. **Pasternak AO, Spaan WJ, Snijder EJ.** 2006. Nidovirus transcription: how to make sense. . .? J. Gen. Virol. **87:**1403–1421.
16. **Snijder EJ, Bredenbeek PJ, Dobbe JC, Thiel V, Ziebuhr J, Poon LL, Guan Y, Rozanov M, Spaan WJ, Gorbalenya AE.** 2003. Unique and conserved features of genome and proteome of SARS-coronavirus, an early split-off from the coronavirus group 2 lineage. J. Mol. Biol. **331:**991–1004.
17. **Perlman S, Netland J.** 2009. Coronaviruses post-SARS: update on replication and pathogenesis. Nat. Rev. Microbiol. **7:**439–450.
18. **Sawicki SG, Sawicki DL, Younker D, Meyer Y, Thiel V, Stokes H, Siddell SG.** 2005. Functional and genetic analysis of coronavirus replicase-transcriptase proteins. PLOS Pathog. **1:**e39. http://dx.doi.org/10.1371/journal.ppat.0010039.
19. **Ulferts R, Imbert I, Canard B, Ziebuhr J.** 2010. Expression and functions of SARS coronavirus replicative proteins, p 75–98. In Lal SK (ed.), Molecular biology of the SARS-coronavirus. Springer Verlag, Berlin, Germany.
20. **Harcourt BH, Jukneliene D, Kanjanahaluethai A, Bechill J, Severson KM, Smith CM, Rota PA, Baker SC.** 2004. Identification of severe acute respiratory syndrome coronavirus replicase products and characterization of papain-like protease activity. J. Virol. **78:**13600–13612.
21. **Prentice E, McAuliffe J, Lu X, Subbarao K, Denison MR.** 2004. Identification and characterization of severe acute respiratory syndrome coronavirus replicase proteins. J. Virol. **78:**9977–9986.
22. **Miller S, Krijnse-Locker J.** 2008. Modification of intracellular membrane structures for virus replication. Nat. Rev. Microbiol. **6:**363–374.
23. **Salonen A, Ahola T, Kääriäinen L.** 2005. Viral RNA replication in association with cellular membranes. Curr. Top. Microbiol. Immunol. **285:**139–173.
24. **den Boon JA, Diaz A, Ahlquist P.** 2010. Cytoplasmic viral replication complexes. Cell Host Microbe **8:**77–85.
25. **den Boon JA, Ahlquist P.** 2010. Organelle-like membrane compartmentalization of positive-strand RNA virus replication factories. Annu. Rev. Microbiol. **64:**241–256.
26. **van Hemert MJ, van den Worm SH, Knoops K, Mommaas AM, Gorbalenya AE, Snijder EJ.** 2008. SARS-coronavirus replication/transcription complexes are membrane-protected and need a host factor for activity in vitro. PLOS Pathog. **4:**e1000054. http://dx.doi.org/10.1371/journal.ppat.1000054.
27. **Netherton CL, Wileman T.** 2011. Virus factories, double membrane vesicles and viroplasm generated in animal cells. Curr. Opin. Virol. **1:**381–387.
28. **Suhy DA, Giddings TH, Kirkegaard K.** 2000. Remodeling the endoplas-

mic reticulum by poliovirus infection and by individual viral proteins: an autophagy-like origin for virus-induced vesicles. J. Virol. **74:**8953–8965.
29. **Stertz S, Reichelt M, Spiegel M, Kuri T, Martínez-Sobrido L, García-Sastre A, Weber F, Kochs G.** 2007. The intracellular sites of early replication and budding of SARS-coronavirus. Virology **361:**304–315.
30. **Gosert R, Kanjanahaluethai A, Egger D, Bienz K, Baker SC.** 2002. RNA replication of mouse hepatitis virus takes place at double-membrane vesicles. J. Virol. **76:**3697–3708.
31. **Hagemeijer MC, Ulasli M, Vonk AM, Reggiori F, Rottier PJ, de Haan CA.** 2011. Mobility and interactions of coronavirus nonstructural protein 4. J. Virol. **85:**4572–4577.
32. **Hagemeijer MC, Verheije MH, Ulasli M, Shaltiël IA, de Vries LA, Reggiori F, Rottier PJ, de Haan CA.** 2010. Dynamics of coronavirus replication-transcription complexes. J. Virol. **84:**2134–2149.
33. **Knoops K, Kikkert M, Worm SH, Zevenhoven-Dobbe JC, van der Meer Y, Koster AJ, Mommaas AM, Snijder EJ.** 2008. SARS-coronavirus replication is supported by a reticulovesicular network of modified endoplasmic reticulum. PLoS Biol. **6:**e226. http://dx.doi.org/10.1371/journal.pbio.0060226.
34. **Snijder EJ, van der Meer Y, Zevenhoven-Dobbe J, Onderwater JJ, van der Meulen J, Koerten HK, Mommaas AM.** 2006. Ultrastructure and origin of membrane vesicles associated with the severe acute respiratory syndrome coronavirus replication complex. J. Virol. **80:**5927–5940.
35. **Ulasli M, Verheije MH, de Haan CA, Reggiori F.** 2010. Qualitative and quantitative ultrastructural analysis of the membrane rearrangements induced by coronavirus. Cell. Microbiol. **12:**844–861.
36. **Prentice E, Jerome WG, Yoshimori T, Mizushima N, Denison MR.** 2004. Coronavirus replication complex formation utilizes components of cellular autophagy. J. Biol. Chem. **279:**10136–10141.
37. **Reggiori F, de Haan CA, Molinari M.** 2011. Unconventional use of LC3 by coronaviruses through the alleged subversion of the ERAD tuning pathway. Viruses **3:**1610–1623.
38. **Knoops K, Swett-Tapia C, van den Worm SH, Te Velthuis AJ, Koster AJ, Mommaas AM, Snijder EJ, Kikkert M.** 2010. Integrity of the early secretory pathway promotes, but is not required for, severe acute respiratory syndrome coronavirus RNA synthesis and virus-induced remodeling of endoplasmic reticulum membranes. J. Virol. **84:**833–846.
39. **van den Worm SH, Knoops K, Zevenhoven-Dobbe JC, Beugeling C, van der Meer Y, Mommaas AM, Snijder EJ.** 2011. Development and RNA-synthesizing activity of coronavirus replication structures in the absence of protein synthesis. J. Virol. **85:**5669–5673.
40. **Posthuma CC, Pedersen KW, Lu Z, Joosten RG, Roos N, Zevenhoven-Dobbe JC, Snijder EJ.** 2008. Formation of the arterivirus replication/transcription complex: a key role for nonstructural protein 3 in the remodeling of intracellular membranes. J. Virol. **82:**4480–4491.
41. **Snijder EJ, van Tol H, Roos N, Pedersen KW.** 2001. Non-structural proteins 2 and 3 interact to modify host cell membranes during the formation of the arterivirus replication complex. J. Gen. Virol. **82:**985–994.
42. **Pedersen KW, van der Meer Y, Roos N, Snijder EJ.** 1999. Open reading frame 1a-encoded subunits of the arterivirus replicase induce endoplasmic reticulum-derived double-membrane vesicles which carry the viral replication complex. J. Virol. **73:**2016–2026.
43. **Baliji S, Cammer SA, Sobral B, Baker SC.** 2009. Detection of nonstructural protein 6 in murine coronavirus-infected cells and analysis of the transmembrane topology by using bioinformatics and molecular approaches. J. Virol. **83:**6957–6962.
44. **Oostra M, Hagemeijer MC, van Gent M, Bekker CP, te Lintelo EG, Rottier PJ, de Haan CA.** 2008. Topology and membrane anchoring of the coronavirus replication complex: not all hydrophobic domains of nsp3 and nsp6 are membrane spanning. J. Virol. **82:**12392–12405.
45. **Barretto N, Jukneliene D, Ratia K, Chen Z, Mesecar AD, Baker SC.** 2005. The papain-like protease of severe acute respiratory syndrome coronavirus has deubiquitinating activity. J. Virol. **79:**15189–15198.
46. **Imbert I, Snijder EJ, Dimitrova M, Guillemot JC, Lécine P, Canard B.** 2008. The SARS-coronavirus PLnc domain of nsp3 as a replication/transcription scaffolding protein. Virus Res. **133:**136–148.
47. **Kanjanahaluethai A, Chen Z, Jukneliene D, Baker SC.** 2007. Membrane topology of murine coronavirus replicase nonstructural protein 3. Virology **361:**391–401.
48. **Neuman BW, Joseph JS, Saikatendu KS, Serrano P, Chatterjee A, Johnson MA, Liao L, Klaus JP, Yates JR, Wüthrich K, Stevens RC, Buchmeier MJ, Kuhn P.** 2008. Proteomics analysis unravels the functional repertoire of coronavirus nonstructural protein 3. J. Virol. **82:**5279–5294.
49. **von Brunn A, Teepe C, Simpson JC, Pepperkok R, Friedel CC, Zimmer R, Roberts R, Baric R, Haas J.** 2007. Analysis of intraviral protein-protein interactions of the SARS coronavirus ORFeome. PLoS One **2:**e459. http://dx.doi.org/10.1371/journal.pone.0000459.
50. **Clementz MA, Kanjanahaluethai A, O'Brien TE, Baker SC.** 2008. Mutation in murine coronavirus replication protein nsp4 alters assembly of double membrane vesicles. Virology **375:**118–129.
51. **Gadlage MJ, Sparks JS, Beachboard DC, Cox RG, Doyle JD, Stobart CC, Denison MR.** 2010. Murine hepatitis virus nonstructural protein 4 regulates virus-induced membrane modifications and replication complex function. J. Virol. **84:**280–290.
52. **Oostra M, te Lintelo EG, Deijs M, Verheije MH, Rottier PJ, de Haan CA.** 2007. Localization and membrane topology of coronavirus nonstructural protein 4: involvement of the early secretory pathway in replication. J. Virol. **81:**12323–12336.
53. **Sparks JS, Lu X, Denison MR.** 2007. Genetic analysis of murine hepatitis virus nsp4 in virus replication. J. Virol. **81:**12554–12563.
54. **Beachboard DC, Lu X, Baker SC, Denison MR.** 2013. Murine hepatitis virus nsp4 N258T mutants are not temperature-sensitive. Virology **435:**210–213.
55. **Cottam EM, Maier HJ, Manifava M, Vaux LC, Chandra-Schoenfelder P, Gerner W, Britton P, Ktistakis NT, Wileman T.** 2011. Coronavirus nsp6 proteins generate autophagosomes from the endoplasmic reticulum via an omegasome intermediate. Autophagy **7:**1335–1347.
56. **Cornillez-Ty CT, Liao L, Yates JR, Kuhn P, Buchmeier MJ.** 2009. Severe acute respiratory syndrome coronavirus nonstructural protein 2 interacts with a host protein complex involved in mitochondrial biogenesis and intracellular signaling. J. Virol. **83:**10314–10318.
57. **Pan J, Peng X, Gao Y, Li Z, Lu X, Chen Y, Ishaq M, Liu D, Dediego ML, Enjuanes L, Guo D.** 2008. Genome-wide analysis of protein-protein interactions and involvement of viral proteins in SARS-CoV replication. PLoS One **3:**e3299. http://dx.doi.org/10.1371/journal.pone.0003299.
58. **Giansanti MG, Belloni G, Gatti M.** 2007. Rab11 is required for membrane trafficking and actomyosin ring constriction in meiotic cytokinesis of Drosophila males. Mol. Biol. Cell **18:**5034–5047.
59. **Schmidt KN, Kuhns S, Neuner A, Hub B, Zentgraf H, Pereira G.** 2012. Cep164 mediates vesicular docking to the mother centriole during early steps of ciliogenesis. J. Cell Biol. **199:**1083–1101.
60. **Verheije MH, Raaben M, Mari M, Te Lintelo EG, Reggiori F, van Kuppeveld FJ, Rottier PJ, de Haan CA.** 2008. Mouse hepatitis coronavirus RNA replication depends on GBF1-mediated ARF1 activation. PLOS Pathog. **4:**e1000088. http://dx.doi.org/10.1371/journal.ppat.1000088.
61. **Kanjanahaluethai A, Baker SC.** 2000. Identification of mouse hepatitis virus papain-like proteinase 2 activity. J. Virol. **74:**7911–7921.